NASA-CR-204654

R-0

Pergamon

0956-7151(95)00374-6

Acta mater. Vol. 44, No. 7, pp. 2809–2820, 1996

Published by Elsevier Science Ltd
Printed in Great Britain. All rights reserved
1359-6454/96 $15.00 + 0.00

NDB
IN-76-CR
([illegible])
030057

CRYSTALLOGRAPHY OF THE NiHfSi PHASE IN A NiAl(0.5 Hf) SINGLE-CRYSTAL ALLOY

A. GARG[1], **R. D. NOEBE**[1] **and R. DAROLIA**[2]
[1]NASA Lewis Research Center, Cleveland, OH 44135 and [2]General Electric Aircraft Engines, Cincinnati, OH 45215, U.S.A.

(Received 25 May 1995; in revised form 18 September 1995)

Abstract—Small additions of Hf to conventionally processed NiAl single crystals result in the precipitation of a high density of cuboidal G-phase along with a newly identified silicide phase. Both of these phases form in the presence of Si which is not an intentional alloying addition but is a contaminant resulting from contact with the ceramic shell molds during directional solidification of the single-crystal ingots. The morphology, crystal structure and orientation relationship (O.R.) of the silicide phase in a NiAl(0.5 at.%Hf) single-crystal alloy have been determined using transmission electron microscopy, electron microdiffraction and energy dispersive X-ray spectroscopy. Qualitative elemental analysis and indexing of the electron microdiffraction patterns from the new phase indicate that it is an orthorhombic NiHfSi phase with unit cell parameters, $a = 0.639$ nm, $b = 0.389$ nm and $c = 0.72$ nm, and space group Pnma. The NiHfSi phase forms as thin rectangular plates on $\{111\}_{\mathrm{NiAl}}$ planes with an O.R. that is given by $(100)_{\mathrm{NiHfSi}} \parallel (111)_{\mathrm{NiAl}}$ and $[010]_{\mathrm{NiHfSi}} \parallel [\bar{1}01]_{\mathrm{NiAl}}$. Twelve variants of the NiHfSi phase were observed in the alloy and the number of variants and rectangular morphology of NiHfSi plates are consistent with symmetry requirements. Quenching experiments indicate that nucleation of the NiHfSi phase in NiAl(Hf) alloys is aided by the formation of $\langle 111\rangle_{\mathrm{NiAl}}$ vacancy loops that form on the $\{111\}_{\mathrm{NiAl}}$ planes. *Copyright © 1996 Acta Metallurgica Inc.*

1. INTRODUCTION

The B2 ordered intermetallic NiAl has long been recognized as a potential candidate material for high-temperature structural applications. Compared to Ni-base superalloys, its lower density (~ 5.9 g/cm^3), higher melting temperature (~ 1955 K), 4–8 fold advantage in thermal conductivity, and its excellent environmental resistance, demonstrated by the fact that nickel aluminide coatings are routinely used to protect superalloys, make it a promising replacement for conventional high-temperature materials [1]. This is particularly true in gas turbine engines where the physical property advantages result in large payoffs in performance. However, NiAl alloys at least in polycrystalline form cannot compete with the superalloys in terms of creep strength or low temperature fracture resistance. Consequently, one approach to solving these problems has been the development of single crystal NiAl alloys [2].

Small additions of alloying elements from groups IVA and VA, in particular Hf and Zr, have been found to be very effective in improving the high-temperature creep strength of NiAl single crystals [2, 3]. These elements provide strengthening by solid-solution effects and precipitate hardening. The latter is believed to be due to nucleation of G-phase ($Ni_{16}Hf_6Si_7$ or $Ni_{16}Zr_6Si_7$), which after prolonged aging at high temperatures may be replaced by a Heusler (β'-Ni_2AlHf or Ni_2AlZr) phase. It should be noted that silicon is not an intentional alloying addition in these materials but enters the melt through reaction with the ceramic shell molds during directional solidification of the single-crystal ingots.

NiAl is an ordered intermetallic compound with a primitive cubic CsCl type structure (space group $Pm\bar{3}m$) and a lattice parameter, $a = 0.289$ nm [1]. The G-phase has a f.c.c. structure (space group $Fm\bar{3}m$) and a lattice parameter, $a = 1.14$ nm, which is almost four times greater than that of NiAl. Consequently, the G-phase is almost coherent with the NiAl matrix and nucleates with a cuboidal morphology and a cube-on-cube orientation relationship (O.R.), i.e. $(100)_G \parallel (100)_{\mathrm{NiAl}}$ and $[010]_G \parallel [010]_{\mathrm{NiAl}}$ [4]. In addition to the G-phase, another morphologically distinct phase was shown to nucleate in a 0.3 at.% Hf containing NiAl single crystal (Fig. 4 in Ref. [4]), however, this phase was not previously identified. This unknown phase was significantly larger in size and appeared to have a lower density as compared to that of the G-phase. In this study, NiAl single crystals containing 0.5 at.% Hf were found to contain the same unknown phase along with the G-phase. This unknown phase has now been identified and details of its crystal structure, morphology and O.R. with NiAl are reported. Additional experiments have been conducted to understand the nucleation characteristics of this phase, the results of which are also described in this paper.

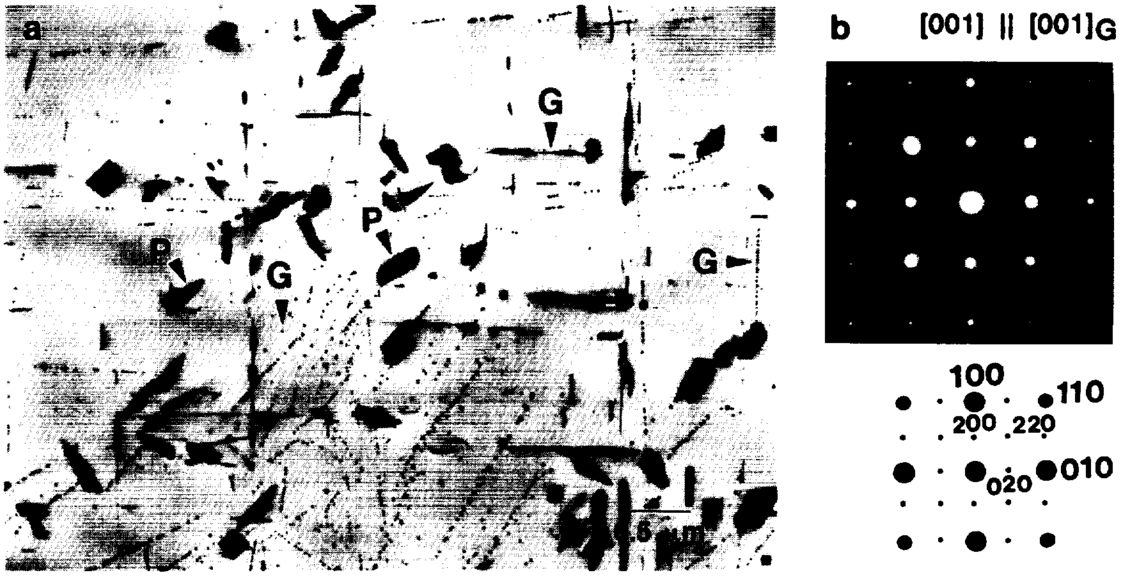

Fig. 1. (a) Bright-field TEM image close to a $\langle 001 \rangle_{NiAl}$ zone-axis showing precipitation of fine G-phase (marked G) and a coarse unknown phase (marked P); (b) the corresponding SADP showing the O.R. between the G-phase and the NiAl matrix.

2. EXPERIMENTAL

A directionally solidified NiAl single crystal containing 0.5 at.% Hf, and other alloying additions in trace amounts (alloy designation D218†) was grown by a Bridgman technique by General Electric Aircraft Engines (GEAE) in the form of a rectangular ingot with approximately (38 × 25)mm^2 cross-section and 96 mm length. The particular ingot, identified as D218-2069, used in this study also contained 0.3 at.% Si due to reaction between the molten metal and ceramic shell mold during directional solidification. The thermal treatment of the ingot consisted of a solution heat treatment of 32 h at 1644 K followed by hot isostatic pressing, and finally a multi-step aging treatment of 0.5 h at 1644 K, 6 h at 1255 K followed by furnace cooling under an argon atmosphere. Cylindrical compression samples for testing along a $\langle 001 \rangle$ orientation were machined from the thermally treated ingot and tested to a maximum of 1% strain at temperatures between 298 and 1300 K. The results of the mechanical testing will be reported in a future paper. Microstructures of the as-thermally treated (i.e. as-received) and compression tested samples have been examined using Transmission Electron Microscopy (TEM). The unknown phase was found to be present in the as-received as well as all compression tested samples, tested to temperatures as high as 1300 K. Although most of this study regarding the unknown phase was conducted on the as-received material, some micrographs have been taken from the compression tested samples.

Slices for TEM were sectioned from 3 mm diameter cylinders machined from the as-received and tested samples. These were mechanically ground and electropolished in a twin-jet Tenupol-3 polisher using a solution of 70% ethanol, 14% distilled water, 10% butylcellosolve and 6% perchloric acid cooled to 263 K. An applied potential of 20–25 V with a corresponding current of 10–15 mA produced electron transparent foils. Microstructural examination, trace analysis and energy dispersive X-ray spectroscopy (EDXS) were carried out in a Philips 400T TEM equipped with a double-tilt goniometer and a KEVEX Si/Li X-ray detector.

3. RESULTS

The microstructure of the as-received material close to a $\langle 001 \rangle_{NiAl}$ zone-axis is shown in Fig. 1(a).

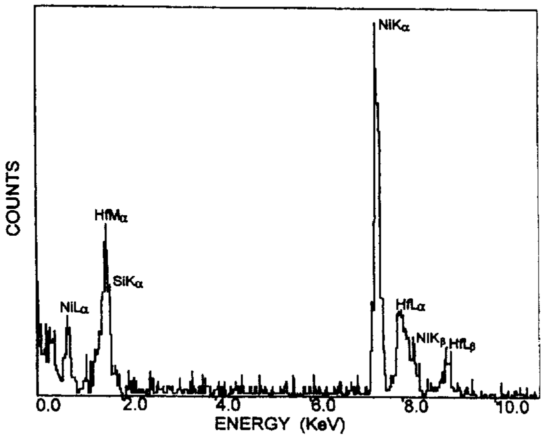

Fig. 2. EDXS spectrum showing the unknown phase to contain Ni, Hf and Si.

---

†The exact chemical composition of the alloy D218 is GEAE proprietary information.

The microstructure consisted of two types of precipitates with a distinct size and morphology difference. The very fine precipitates of size ~5–50 nm, had a cuboidal morphology and a $\{100\}_{NiAl}$ habit plane and were identified as the G-phase precipitates from the selected-area diffraction pattern (SADP) [Fig. 1(b)]. Some of the G-phase precipitates on edge-on $\{100\}_{NiAl}$ planes also showed a plate shape morphology. The second type of precipitates, marked P in Fig. 1(a), were inclined with respect to the beam,

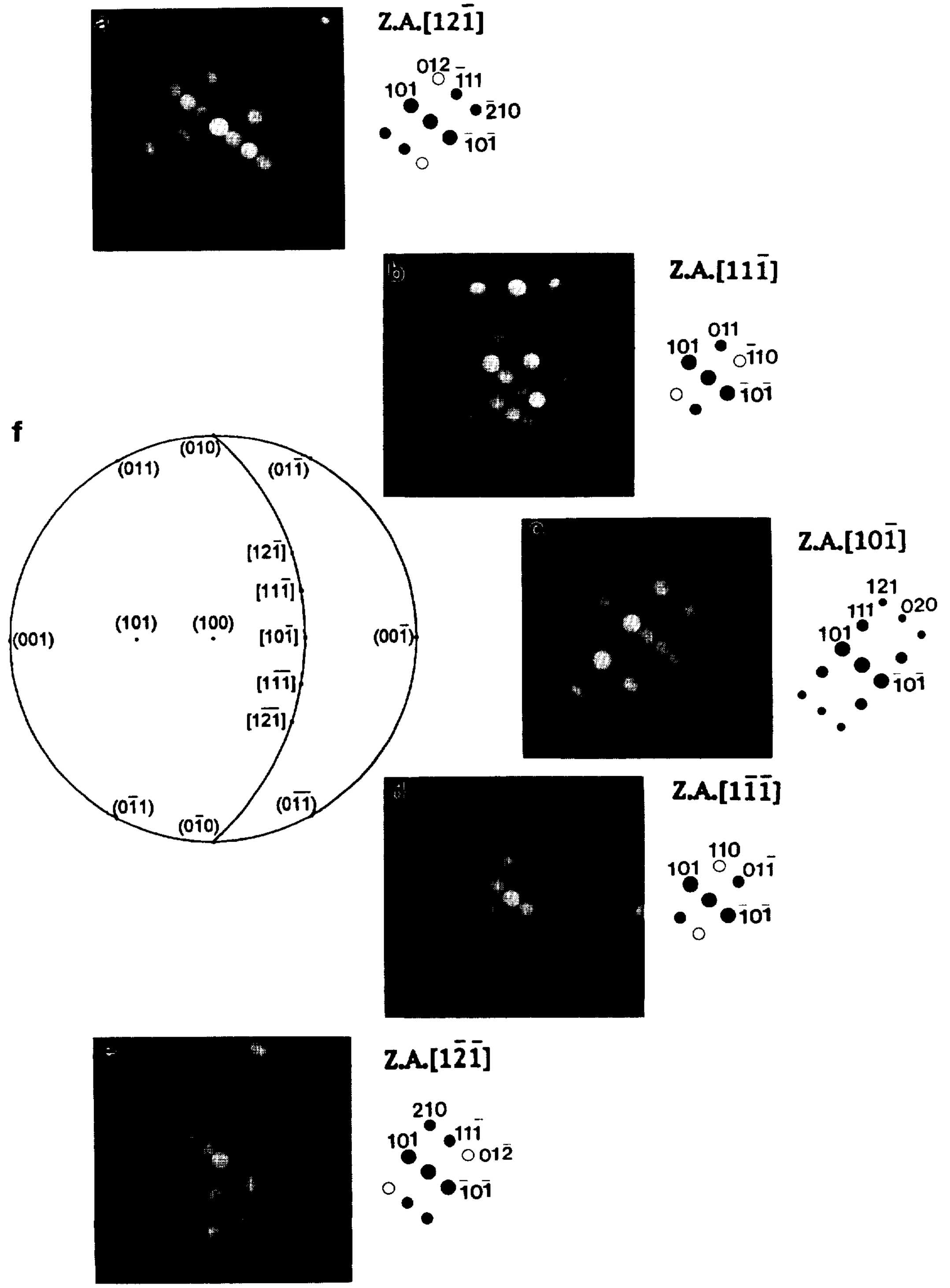

Fig. 3. Sequential MBED patterns from a single precipitate in (a) [12$\bar{1}$]; (b) [11$\bar{1}$]; (c) [10$\bar{1}$]; (d) [1$\bar{1}\bar{1}$]; and (e) [1$\bar{2}\bar{1}$] zone-axis. The corresponding stereographic projection in (f) shows these zone-axes for the orthorhombic NiHfSi structure. Double diffraction spots are shown by "o".

had a larger size (~200–500 nm), and a distinctly different morphology from that of the G-phase precipitates. The density of this phase was much lower than that of the G-phase precipitates and its distribution was non-uniform throughout the microstructure. EDXS showed that these larger precipitates were rich in Hf and Ni and contained some Si (Fig. 2). It should be noted that in the presence of Hf, an unambiguous determination of Si is not always possible due to proximity of the SiK$_\alpha$ (1.745 keV) and HfM$_\alpha$ (1.645 keV) energy peaks. However, in Fig. 2 the broad HfM$_\alpha$ peak and the asymmetrical shoulder

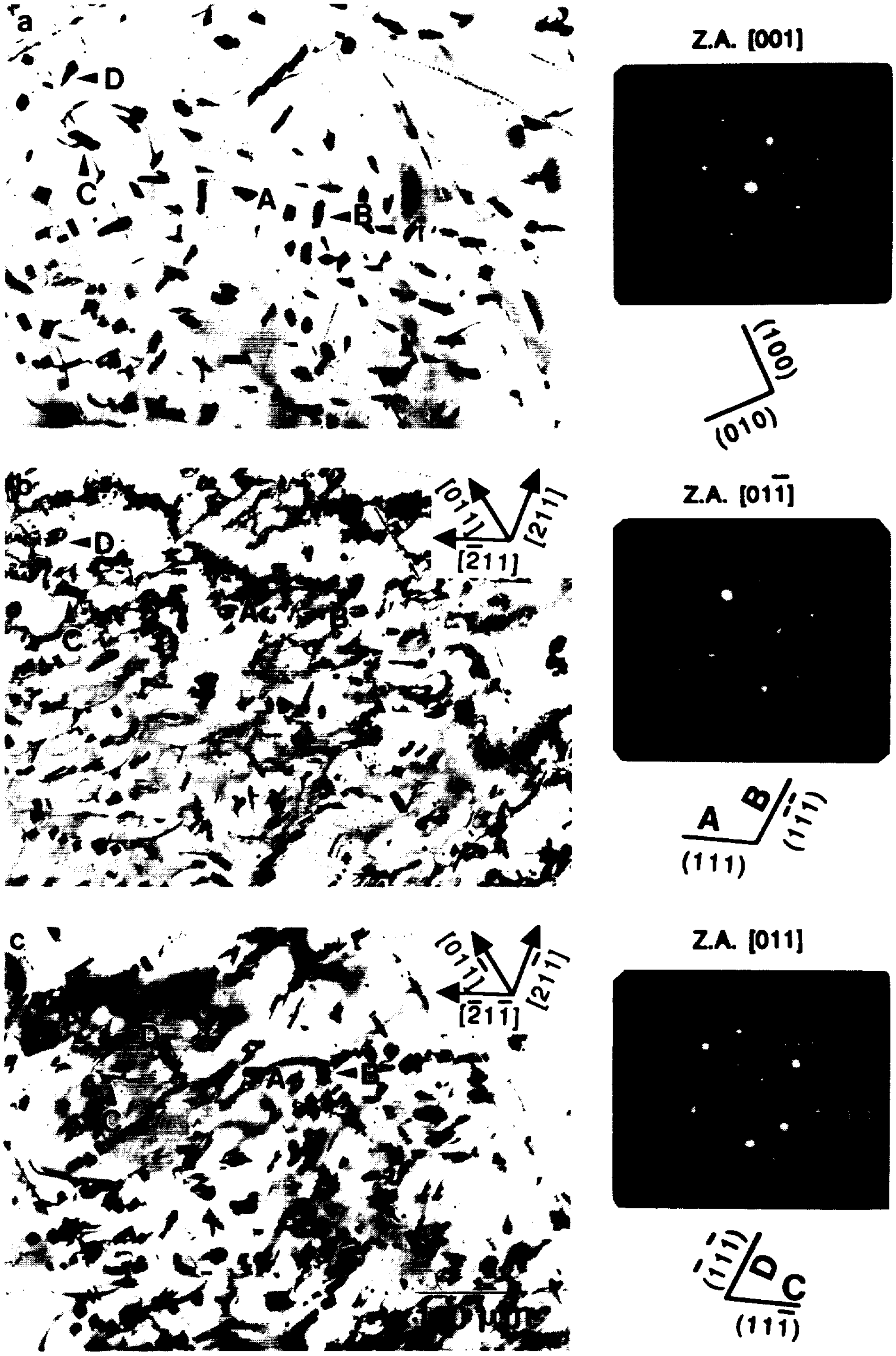

Fig. 4. Bright-field TEM images of the same area close to the zone-axis (a) [001]; (b) [01$\bar{1}$]; and (c) [011], showing edge-on NiHfSi precipitates on $\{111\}_{NiAl}$ planes.

on the right-hand side of the peak suggest the presence of Si in the precipitate.

To identify the crystal structure of these larger unknown precipitates, a low-index microbeam electron-diffraction (MBED) pattern, sown in Fig. 3(a), was obtained from one of the precipitates. Within the accuracy of measurement, this pattern could be best indexed as the $[12\bar{1}]$ zone-axis pattern for the orthorhombic NiHfSi phase with unit-cell parameters $a = 0.639$ nm, $b = 0.389$ nm and $c = 0.72$ nm, having space group Pnma [5] (Co_2Si structure, space group no. 62 [6]). Since this phase had not been reported previously in a NiAl alloy, confirmation of this structure through several zone-axes patterns was considered essential. Therefore, a series of low index MBED patterns was recorded in sequence from a single precipitate such that the set of planes indexed as (101) in Fig. 3(a) was always diffracting. The patterns thus obtained are shown in Figs 3(a)–(e) and were consistently indexed as the $[12\bar{1}]$, $[11\bar{1}]$, $[10\bar{1}]$, $[1\bar{1}\bar{1}]$ and $[1\bar{2}\bar{1}]$ zone-axis patterns for the orthorhombic NiHfSi structure. These zone-axes sequentially lie

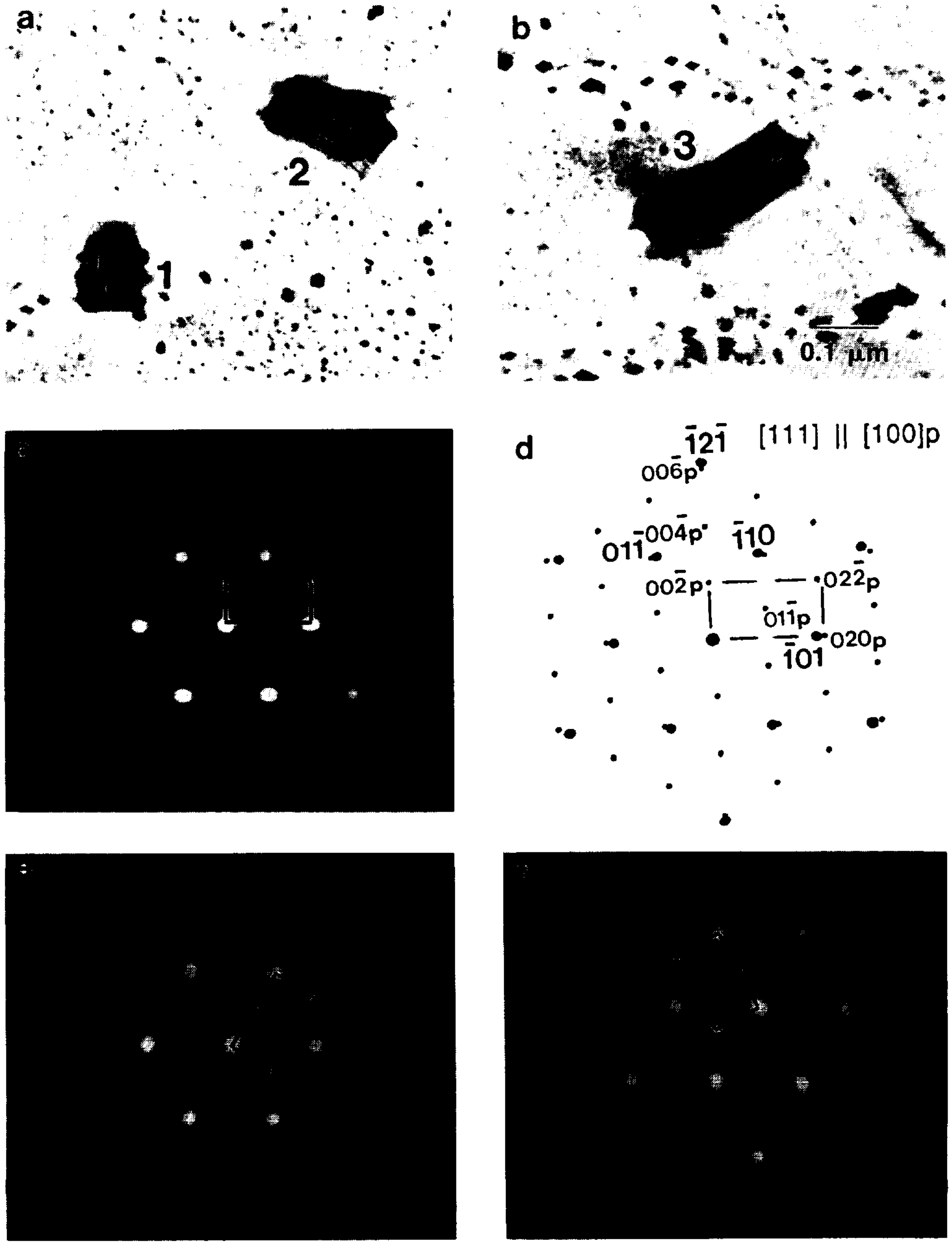

Fig. 5. (a), (b) TEM micrographs showing three variants of the NiHfSi phase (marked 1,2,3) in a $\{111\}_{NiAl}$ plane; (c), (e), (f) the corresponding MBED patterns distinguishing the three variants; (d) schematic solution of (c) showing Z. A. $[111]_{NiAl} \| [100]_{NiHfSi(P)}$.

on the great circle of the pole $(101)_{\text{NiHfSi}}$ for the orthorhombic NiHfSi crystal structure, as shown in the stereographic projection in Fig. 3(f). MBED patterns were recorded and analyzed from several of the larger precipitates, verifying that they all consisted of the same orthorhombic structure. Although the MBED patterns confirmed this phase to be the orthorhombic NiHfSi, the exact stoichiometry of the phase by quantitative EDX microanalysis was not determined.

To find the habit plane of these precipitates, a tilting experiment was conduced which revealed that the NiHfSi precipitates became edge-on in $\langle 011\rangle_{\text{NiAl}}$ zone-axes. Four sets of inclined plates in the $[001]_{\text{NiAl}}$ orientation were marked A, B, C and D in Fig. 4(a). In the $[01\bar{1}]_{\text{NiAl}}$ orientation, sets of plates A and B were edge-on and parallel to the beam, whereas the plates belonging to the sets C and D were inclined 35° with respect to the beam [Fig. 4(b)]. Trace analysis indicated that sets of plates A and B had habit planes $(111)_{\text{NiAl}}$ and $(\bar{1}11)_{\text{NiAl}}$, respectively. Similarly, in the $[011]_{\text{NiAl}}$ orientation [Fig. 4(c)], sets of plates C and D were parallel to the beam and had habit planes $(11\bar{1})_{\text{NiAl}}$ and $(1\bar{1}1)_{\text{NiAl}}$, respectively. Thus, the orthorhombic NiHfSi phase was formed on all four $\{111\}_{\text{NiAl}}$ planes. This is in contrast to the f.c.c. G-phase that formed on $\{100\}_{\text{NiAl}}$ planes. Due to different habit planes, NiHfSi and G-phases can be distinguished easily in a $\langle 110\rangle_{\text{NiAl}}$ zone-axis from their traces, which lie along $\langle 112\rangle_{\text{NiAl}}$ and $\langle 110\rangle_{\text{NiAl}}$ directions, respectively [Figs 4(b) and (c)]. Likewise, their distinction is also easier in a $\langle 001\rangle_{\text{NiAl}}$ zone-axis, where the G-precipitates are either parallel or normal to the beam, whereas the NiHfSi phase is always inclined with respect to the beam [Fig. 1(a)].

The thickness of the edge-on NiHfSi plates was very small (~30–60 nm) compared to their length (200–500 nm), suggesting restricted growth normal to the habit plane. When viewed along a $\langle 111\rangle_{\text{NiAl}}$ direction, NiHfSi precipitate plates fully contained in the foil thickness exhibited a rectangular morphology, as shown in Figs 5(a) and (b). Since the density of G-phase was very high compared to that of the NiHfSi phase, a general SADP showed intense diffraction spots from the NiAl matrix and the G-phase and very faint spots from the NiHfSi phase. Therefore, the O.R. between the NiHfSi precipitate and the NiAl matrix was obtained from the MBED patterns. The MBED pattern obtained from a flat-on precipitate plate with a habit plane $(111)_{\text{NiAl}}$ normal to the beam, is shown in Fig. 5(c). This pattern was indexed as the [100] zone-axis pattern for the orthorhombic NiHfSi phase [Fig. 5(d)], and the O.R. obtained from Figs 5(c) and (d), which also shows the

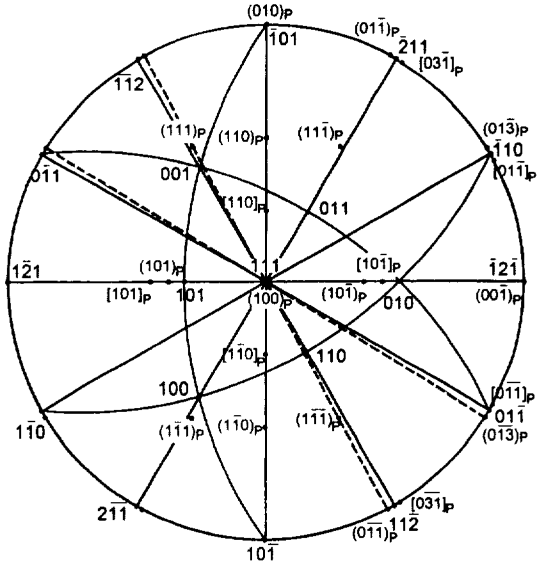

Fig. 6. Stereographic projection showing the orientation relationship between the orthorhombic NiHfSi phase (P) and the cubic NiAl matrix.

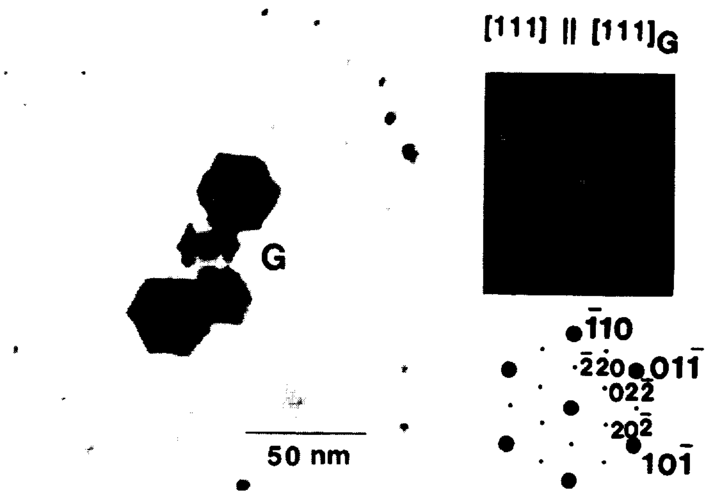

Fig. 7. Projected hexagonal morphology and observed MBED and simulated SADP patterns from a cuboidal G-phase precipitate along a $\langle 111\rangle_{\text{NiAl}} \| \langle 111\rangle_{G}$ direction.

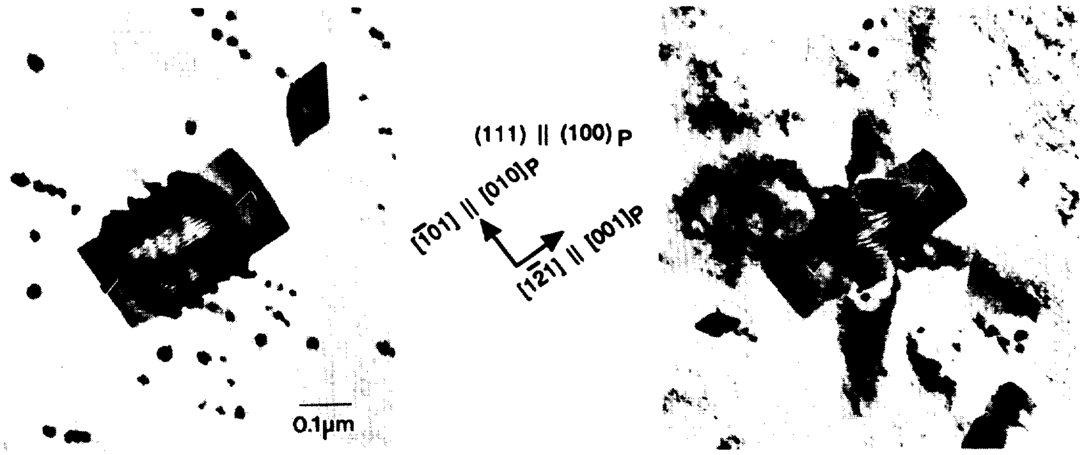

Fig. 8. TEM micrographs close to a $\langle 111\rangle_{NiAl}$ zone-axis, showing growth ledges (arrowed) on the faces of NiHfSi precipitate plates.

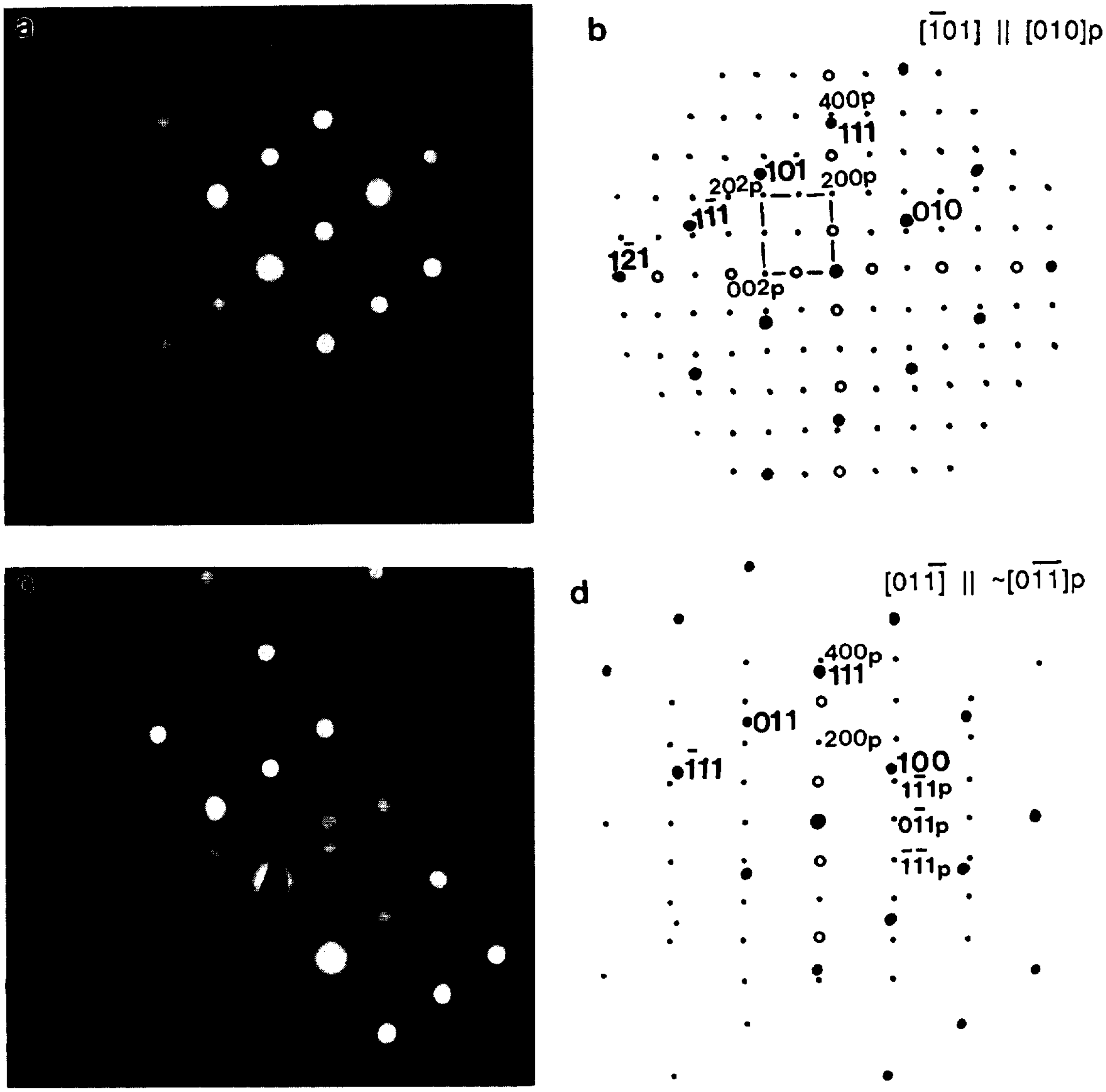

Fig. 9. (a-d)—*Caption* overleaf.

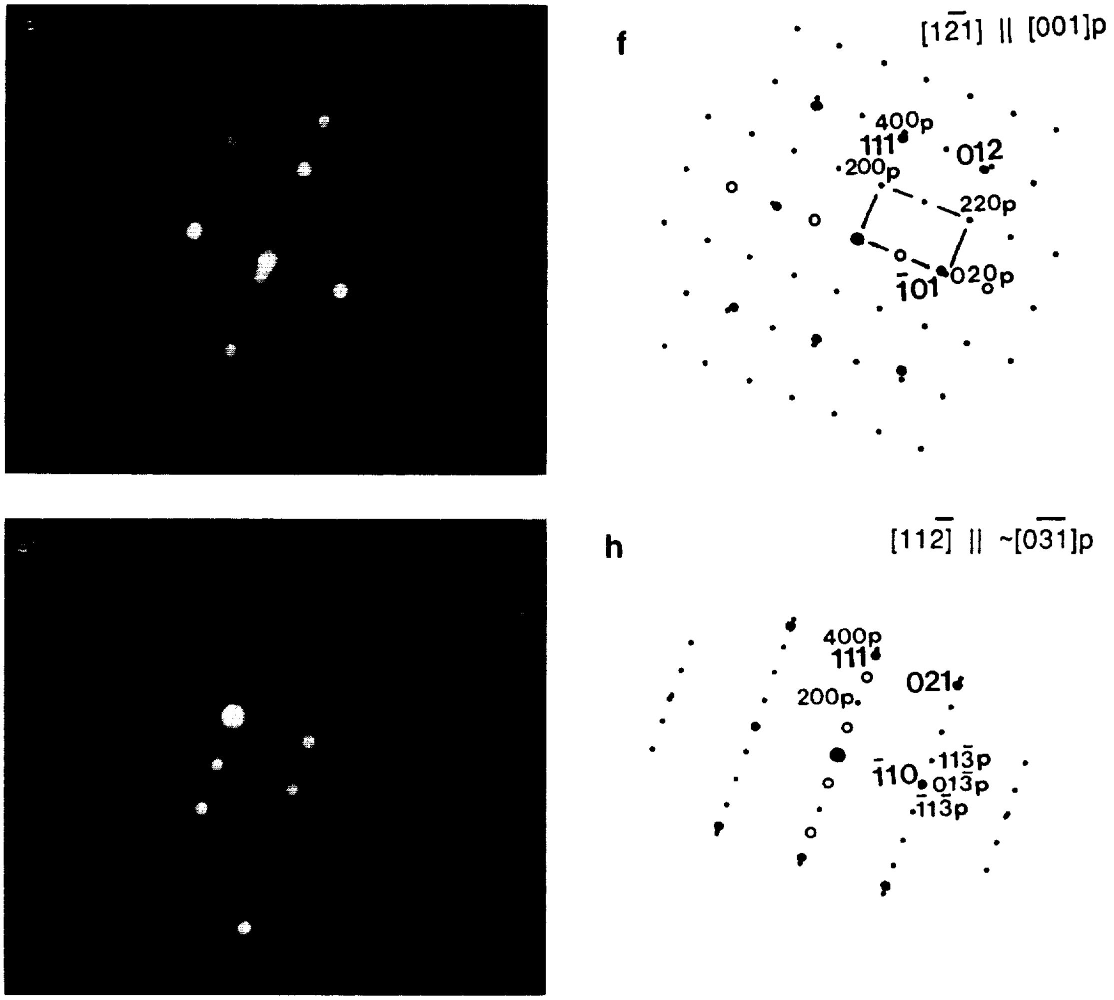

Fig. 9(e–h)

Fig. 9. Observed MBED, and simulated SADP patterns from large edge-on NiHfSi precipitate plates observed in a compression tested sample, parallel to (a)–(d) $\langle 110\rangle_{NiAl}$ zone-axis; (e)–(h) $\langle 112\rangle_{NiAl}$ zone-axis. Double diffraction spots are shown by "o".

superimposed $[111]_{NiAl}$ zone-axis MBED pattern of the NiAl matrix, is given by:

$$(100)_{NiHfSi} \parallel (111)_{NiAl}$$

$$[010]_{NiHfSi} \parallel [\bar{1}01]_{NiAl}$$

$$[001]_{NiHfSi} \parallel [1\bar{2}1]_{NiAl}.$$

This O.R. is illustrated in the stereographic projection in Fig. 6. Since there is a 3-fold symmetry about the $\langle 111\rangle_{NiAl}$ axis, there are three equivalent $\langle 110\rangle_{NiAl}$ directions in each $\{111\}_{NiAl}$ plane and hence three possible variants of the NiHfSi phase in each habit plane. For example, in the $(111)_{NiAl}$ plane, the $[010]_{NiHfSi}$ axis may be parallel to either of the three $[\bar{1}01]$, $[0\bar{1}1]$ or $[1\bar{1}0]$ NiAl directions. All three variants were experimentally observed and the MBED patterns obtained from each of the three variants marked 1, 2 and 3 in Figs 5(a) and (b) are shown in Figs 5(c), (e) and (f), respectively. The morphology of the plates was rectangular in each case and Moiré fringes associated with the $\{101\}_{NiAl}$ ($d = 0.204$ nm) and $(020)_{NiHfSi}$ ($d = 0.195$ nm) reflections were clearly visible running perpendicular to $g\langle 101\rangle_{NiAl} \parallel g[010]_{NiHfSi}$. In each variant, the preferential growth in the plane of the plate was found to be along the $[001]_{NiHfSi} \parallel \langle 121\rangle_{NiAl}$ direction. In contrast, the cuboidal G-phase precipitates when viewed along a $\langle 111\rangle_{NiAl} \parallel \langle 111\rangle_G$ direction exhibit a hexagonal morphology and a distinctly different MBED pattern, as shown in Fig. 7.

Growth ledges leading to thickening of the NiHfSi precipitate plates were frequently observed on the plate faces. An unusual ledge source observed in some of the plates was the center of the platelets where a pair of ledges seemed to nucleate and migrate laterally in the $\langle 121\rangle_{NiAl} \parallel [001]_{NiHfSi}$ direction from either side of the plate center. Typical examples of this unusual morphology of growth ledges are shown in Fig. 8.

The O.R. predicted along $\langle 110\rangle_{NiAl}$ and $\langle 112\rangle_{NiAl}$ zone-axes in Fig. 6 was also verified experimentally. In a $\langle 110\rangle_{NiAl}$ zone-axis, two sets of plates have their habit planes parallel to the electron beam [Figs 4(b) and (c)]. Microdiffraction patterns were obtained from a number of edge-on plates belonging to each set and it was found that only two distinct patterns were obtained in each case. These patterns are shown in Figs 9(a) and (c) and were indexed as the $[010]_{\mathrm{NiHfSi}}$ [Fig. 9(b)] and $[001]/[01\bar{1}]_{\mathrm{NiHfSi}}$ [Fig. 9(d)] zone-axis patterns, respectively. This is also predicted from the stereographic projection of Fig. 6, where in the $[\bar{1}01]_{\mathrm{NiAl}}$ direction, only one of the three possible variants is expected to have $[010]_{\mathrm{NiHfSi}} \parallel [\bar{1}01]_{\mathrm{NiAl}}$, whereas the other two variants will have [011] or $[01\bar{1}]_{\mathrm{NiHfSi}}$ parallel (within 1.6°) to the beam and thus be indistinguishable. In a $\langle 112\rangle_{\mathrm{NiAl}}$ zone-axis, only one type of $\{111\}_{\mathrm{NiAl}}$ plane is edge-on and therefore, only one array of NiHfSi plates have their habit plane parallel to the electron beam. In this orientation, only two distinct patterns were again observed from a number of edge-on plates [Figs 9(e) and (g)]. These patterns could be indexed as either the $[001]_{\mathrm{NiHfSi}}$ [Fig. 9(f)] or the $[03\bar{1}]/[031]_{\mathrm{NiHfSi}}$ [Fig. 9(h)] zone-axis patterns. This is again consistent with the orientation relationship depicted in the stereographic projection where in the $[\bar{1}2\bar{1}]_{\mathrm{NiAl}}$ orientation, only one variant of NiHfSi is expected to have its [001] axis parallel to the beam whereas the other two would be indistinguishable and will have their [031] or $[03\bar{1}]$ axes parallel (within 1.6°) to the beam (Fig. 6). The small deviation of the $[011]/[01\bar{1}]_{\mathrm{NiHfSi}}$ and $[03\bar{1}]/[031]_{\mathrm{NiHfSi}}$ zone-axes from the respective $\langle 110\rangle_{\mathrm{NiAl}}$ and $\langle 112\rangle_{\mathrm{NiAl}}$ zone-axes obtained from the O.R. and displayed in the stereographic projection, is also observed in the experimental MBED patterns, as shown in Figs 9(c) and (g), respectively. Since the multiplicity of $\{111\}_{\mathrm{NiAl}}$ planes is four and there are three possible variants per plane, there are 12 crystallographically equivalent variants of the NiHfSi phase in the NiAl matrix.

4. DISCUSSION

In homogenized and aged NiAl(Hf) single crystals, an orthorhombic NiHfSi phase has been identified for the first time. This phase nucleates on $\{111\}_{\mathrm{NiAl}}$ planes as rectangular platelets and co-exists independently of the cuboidal G-phase which has a $\{100\}_{\mathrm{NiAl}}$ habit plane. The electron-diffraction results indicate that there are 12 variants of the NiHfSi phase in the NiAl matrix. The number of possible variants can also be determined solely from symmetry considerations of the precipitate and matrix structures using the method of Cahn and Kalonji [7]. The point group symmetry of NiAl is m3m and of order 48. The orientation relationship in Fig. 6 suggests that the symmetry elements common to the precipitate and the matrix elements are a 2-fold axis ($[010]_{\mathrm{NiHfSi}} \parallel [10\bar{1}]_{\mathrm{NiAl}}$) and the mirror plane m perpendicular to this axis in each phase. The intersection point group is therefore 2/m (monoclinic) and of order 4. The number of variants thus predicted is 48/4 = 12, which is in agreement with the experimental observations. The rectangular morphology of the precipitate plates observed in the habit plane is also compatible with the intersection point group 2/m, since a crystal form consisting of a pair of parallel planar surfaces either perpendicular or parallel to the 2-fold axis is predicted [8] for this common point group.

The stereographic projection showing the orientation relationship between the NiHfSi and the NiAl matrix in Fig. 6 clearly indicates that in the habit plane of the precipitate, i.e. $(100)_{\mathrm{NiHfSi}} \parallel (111)_{\mathrm{NiAl}}$, only two directions (and the planes perpendicular to these directions) are exactly parallel in the precipitate and the matrix phases. These directions are $[010]_{\mathrm{NiHfSi}} \parallel [\bar{1}01]_{\mathrm{NiAl}}$ and $[001]_{\mathrm{NiHfSi}} \parallel [\bar{1}2\bar{1}]_{\mathrm{NiAl}}$. The lattice misfit between the corresponding planes $(010)_{\mathrm{NiHfSi}}$ and $(\bar{1}01)_{\mathrm{NiAl}}$ and $(001)_{\mathrm{NiHfSi}}$ and $(\bar{1}2\bar{1})_{\mathrm{NiAl}}$ is 4.8% and 1.7%, respectively. In the other two $\langle 110\rangle_{\mathrm{NiAl}}$ directions, planes $(\bar{1}10)_{\mathrm{NiAl}}$ and $(01\bar{3})_{\mathrm{NiHfSi}}$ and $(0\bar{1}1)_{\mathrm{NiAl}}$ and $(013)_{\mathrm{NiHfSi}}$ have a misfit of only 0.05% but each pair of planes is misoriented by 1.6°. Similarly, in the other two $\langle 112\rangle_{\mathrm{NiAl}}$ directions in the $(111)_{\mathrm{NiAl}}$ plane, planes $(\bar{2}11)_{\mathrm{NiAl}}$ and $(01\bar{1})_{\mathrm{NiHfSi}}$, and $(11\bar{2})_{\mathrm{NiAl}}$ and $(011)_{\mathrm{NiHfSi}}$ have a misfit of 3.3% and each pair of planes is misoriented by 1.6°. The misfit normal to the precipitate plate, i.e. along $[100]_{\mathrm{NiHfSi}} \parallel [111]_{\mathrm{NiAl}}$ is 4.3%. Thus, in the habit plane of the precipitate plate, the direction of least misfit along which the parallelism between the corresponding planes is also maintained is $[001]_{\mathrm{NiHfSi}} \parallel \langle 112\rangle_{\mathrm{NiAl}}$. Therefore, once a NiHfSi precipitate is formed, the preferred growth of the precipitate plate is expected to occur in the $[001]_{\mathrm{NiHfSi}} \parallel \langle 112\rangle_{\mathrm{NiAl}}$ direction, which is in agreement with the experimental observations. The misfit between the NiHfSi phase and the NiAl matrix in different directions is accommodated by the presence of misfit dislocations which were often observed at the particle–matrix interfaces.

Simultaneous and yet independent nucleation of the semicoherent NiHfSi phase with relatively large misfit along with the nearly coherent G-phase in NiAl(Hf) single crystals is somewhat surprising. Each of these phases is composed of the same elemental constituents (Ni, Hf and Si) but has a very different chemical composition and crystal structure. The density of G-phase is much higher and its size is ~10 times smaller than that of the NiHfSi phase. The nucleation of G-phase is undoubtedly triggered by its good coherency and a small lattice misfit (1.4%) in all three $\langle 100\rangle_{\mathrm{NiAl}}$ directions. The presence of $\langle 100\rangle_{\mathrm{NiAl}}$ dislocations also aids in the preferential nucleation and growth of G-phase [4] since a reduction in strain energy results. On the other hand, the NiHfSi phase is partially coherent and does not possess a low misfit in several of the low-index directions in the plane of the precipitate. Therefore, the driving force for the nucleation of this phase is still not clear but is most likely heterogeneous.

There are at least two factors that can trigger the nucleation of the NiHfSi phase in the presence of G-phase. One is the condensation and collapse of excess vacancies to form $\langle 111 \rangle_{NiAl}$ prismatic loops onto $\{111\}_{NiAl}$ planes, and the other is the segregation and/or clustering of alloying elements on $\{111\}_{NiAl}$ planes. Both of these processes would help in the nucleation of the NiHfSi phase, the former by reducing the strain energy along the $\langle 111 \rangle_{NiAl}$ direction and the latter by reducing the activation energy barrier for nucleation.

The first possibility is rather easy to check since excess vacancy content, and therefore number of $\{111\}_{NiAl}$ dislocation loops, can be controlled by varying the quenching rate and/or the solute content [9]. Therefore, the as-received samples were re-homogenized at 1590 K for 20 h and then quenched into two different media, water and air. The microstructure of the water-quenched sample was almost featureless except for the presence of a small number of concentric dislocation loops that surrounded discrete tiny particles [Fig. 10(a)]. The microstructure of the air-cooled sample contained a

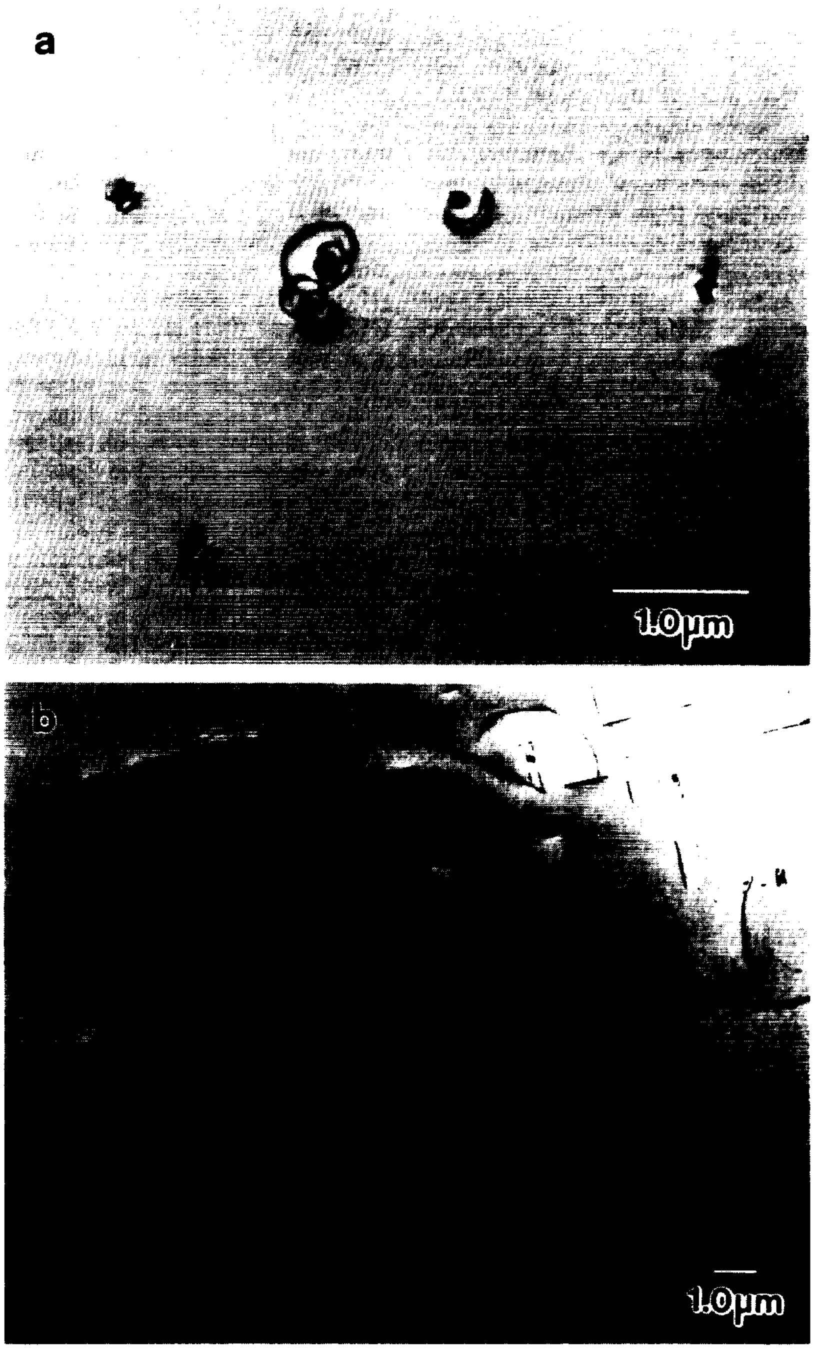

Fig. 10. TEM micrographs showing microstructure of the NiAl(0.5 Hf) alloy after re-homogenization and (a) water quenching, (b) air cooling. Note difference in magnification between the two micrographs.

much higher density of such loops which were also larger in size [Fig. 10(b)]. Each set of concentric loops was again associated with a particle that was observed in the center of the loops and appeared to be the source responsible for nucleating the concentric loops. The loops were identified as prismatic $\langle 100 \rangle_{NiAl}$ dislocation loops that had climbed away from the particle by absorbing vacancies that arrived at the particle–matrix interface during the quench. This process has been described in detail in an accompanying paper [10]. The particles located within the center of each series of loops were identified as the NiHfSi precipitates. These observations suggested that excess vacancies existed in the NiAl(0.5% Hf) alloy, however since the precipitation of NiHfSi phase had already occurred, their nucleation sites could not be identified.

Therefore, an alloy with increased Hf content (1.0 at.%), and reduced Si content (0.1 at.%) was chosen for further experimentation. The rationale was to increase the number of vacancies by increasing the total solute content and at the same time reduce one of the solute species necessary for precipitation of the NiHfSi phase. In other words, increase the driving force for nucleation of the NiHfSi phase and reduce its ability to nucleate in hopes of identifying the heterogeneous nucleation sites. The modified alloy was homogenized at 1590 K for 50 h and then air-cooled. TEM foils prepared from this alloy showed a high density of small dislocation loops along with fine G-phase cuboidal precipitates [Fig. 11(a)]. The loops could be seen clearly in a weak-beam dark-field image shown in Fig. 11(b). In a $\langle 110 \rangle_{NiAl}$ zone-axis, these loops became edge-on and trace analysis indicated that they were formed on the $\{111\}_{NiAl}$ planes [arrows in Fig. 11(c)]. In addition, faint streaking along the $\langle 111 \rangle_{NiAl}$ directions and weak intensity maxima at $\sim 1/4$, $1/2$ and $3/4\, g\langle 111 \rangle_{NiAl}$ positions were also observed in a $\langle 110 \rangle_{NiAl}$ zone-axis SADP [Fig. 11(d)]. In general, the streaking can be associated with thin platelets formed on $\{111\}_{NiAl}$ planes as well as the presence of $\langle 111 \rangle_{NiAl}$ dislocation loops. Extra spots in the SADP should confirm the formation of a second phase in the microstructure. However, in the presence of G-phase, weak spots along $\langle 111 \rangle_{NiAl}$ directions cannot unambiguously be associated with the NiHfSi phase, since the diffraction spots corresponding to both the $\{111\}_G$ ($d_{111} = 0.66$ nm) and the $\{100\}_{NiHfSi}$

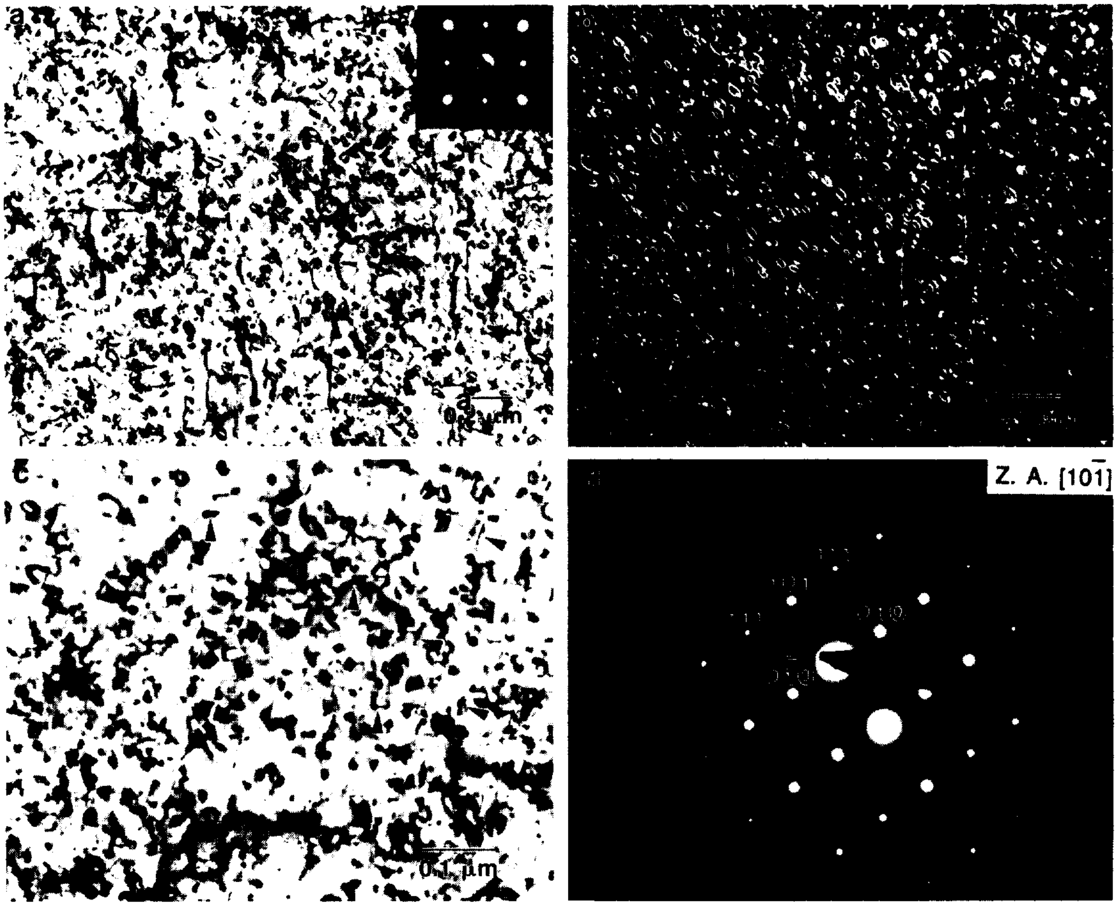

Fig. 11. (a)–(c) TEM micrographs showing the microstructure of homogenized and air-cooled NiAl(1 Hf, 0.1 Si) alloy: (a) $\langle 100 \rangle_{niAl}$ zone-axis image; (b) WBDF image; (c), (d) $\langle 110 \rangle_{NiAl}$ zone-axis image and the corresponding SADP.

($d_{100} = 0.64$ nm) planes lie along $\langle 111 \rangle_{NiAl}$ directions and are very close to each other. Nevertheless, presence of quenched-in $\langle 111 \rangle_{NiAl}$ vacancy loops should provide preferential nucleation sites for the NiHfSi precipitates which have a considerable amount of misfit (4.3%) normal to the $\{111\}_{NiAl}$ habit planes. The driving force for nucleation would be a large reduction in strain energy in the $\langle 111 \rangle_{NiAl} \parallel [100]_{NiHfSi}$ direction.

It is clear from these observations that in NiAl(Hf) alloys, nucleation of the NiHfSi phase is strongly dependent on the supersaturation of vacancies and their condensation during the quench onto $\{111\}_{NiAl}$ planes to form $\langle 111 \rangle_{NiAl}$ dislocation loops. Of course, the availability of solute (Hf and Si) is essential for the precipitation to occur on these loops. Thus, any experimental parameter controlling the excess vacancy concentration and their condensation and collapse on $\{111\}_{NiAl}$ planes can affect the nucleation of this phase. Variation in homogenization heat treatment and quenching rates or addition of alloying elements which have a high solute-vacancy binding energy may prove very effective in controlling the volume fraction of this phase for achieving optimum mechanical properties of NiAl(Hf) single crystals.

5. CONCLUSIONS

(1) A new silicide phase, NiHfSi, has been identified in NiAl(Hf) single-crystals. This phase has an orthorhombic structure ($a = 0.639$ nm, $b = 0.389$ nm, $c = 0.72$ nm; space group Pnma), and a $\{111\}_{NiAl}$ habit plane and nucleates with an orientation relationship with the NiAl matrix defined by $(100)_{NiHfSi} \parallel (111)_{NiAl}$ and $[010]_{NiHfSi} \parallel [\bar{1}01]_{NiAl}$.

(2) The morphology of the NiHfSi precipitates on the {111] planes is rectangular plates with restricted growth perpendicular to the plate along which the misfit is large (4.3%), and preferential growth in the plane of the plate along the $[001]_{NiHfSi}(\parallel \langle 112 \rangle_{NiAl})$ direction along which the misfit is least (1.7%), and parallelism between the corresponding planes is maintained.

(3) Twelve variants of the NiHfSi phase are observed in the NiAl matrix, which is consistent with the symmetry considerations of the matrix and the precipitate crystal structures.

(4) Nucleation of the NiHfSi phase with a $\{111\}_{NiAl}$ habit plane in NiAl(Hf) alloys is apparently aided by $\langle 111 \rangle_{NiAl}$ vacancy loops which form on $\{111\}_{NiAl}$ planes during cooling from the homogenization heat treatment temperature.

Acknowledgements—The authors would like to thank Prof. Ben Oliver of the University of Tennessee for growing the NiAl(1.0 Hf, 0.1 Si) alloy used in the quenching study. Helpful technical discussions with Prof. J. M. Howe of the University of Virginia and his valuable comments on the paper are gratefully acknowledged. Special thanks to Drs Sue Draper and Mike Nathal of the NASA Lewis Research Center for reviewing the paper. This work was performed through a Space Act Agreement with GEAE and was funded by the NASA Advanced High Temperature Engine Materials Technology Program.

REFERENCES

1. R. D. Noebe, R. R. Bowman and M. V. Nathal, *Int. Mater. Rev.* **38,** 193 (1993).
2. R. Darolia, *JOM* **43** (3), 44 (1991).
3. I. E. Locci, R. Dickerson, R. R. Bowman, J. D. Whittenberger, M. V. Nathal and R. Darolia, *Mater. Res. Soc. Symp. Proc.* **288,** 685 (1993).
4. I. E. Locci, R. D. Noebe, R. R. Bowman, R. V. Miner, M. V. Nathal and R. Darolia, *Mater. Res. Soc. Symp. Proc.* **213,** 1013 (1991).
5. P. Villarsm and L. D. Calvert, *Pearson's Handbook of Crystallographic Data for Intermetallic Phases*, p. 3895 ASM International, Materials Park, OH (1991).
6. Theo Hahn, *International Tables for Crystallography*, Vol. A, p. 288. The International Union of Crystallography (1987).
7. J. W. Cahn and G. Kalonji, in *Proc. Int. Conf. on Solid–Solid Phase Transformations* (edited by H. I. Aaronson, R. F. Sekerka, D. E. Laughlin and C. M. Wayman), pp. 3–14. TMS-AIME, Warrendale, PA (1982).
8. M. J. Buerger, *Introduction to Crystal Geometry*. McGraw-Hill, New York (1971).
9. K. H. Westmacott, R. S. Barnes, D. Hull and R. E. Smallman, *Phil. Mag.* **6,** 929 (1961).
10. A. Garg, R. D. Noebe and R. Darolia, to be published.